Supplementary Materials: Magnetically Assisted Separation of Weakly Magnetic Metal Ions in Porous Media.

Part 2: Numerical Simulations

Muhammad Jamiu Garba[1,2], Alwell Nwachukwu[1,2], Jamel Ali[1,2],
Theo Siegrist[1,2], Munir Humayun[2,3], Hadi Mohammadigoushki[1,2,*]

[1]Department of Chemical and Biomedical Engineering, FAMU-FSU College of Engineering, Tallahassee, FL

[2]National High Magnetic Field Laboratory, Tallahassee, FL

[3]Department of Earth, Ocean and Atmospheric Science, Florida State University, Tallahassee, FL

*Corresponding author: hadi.moham@eng.famu.fsu.edu

October 29, 2025

Additional Simulation Results

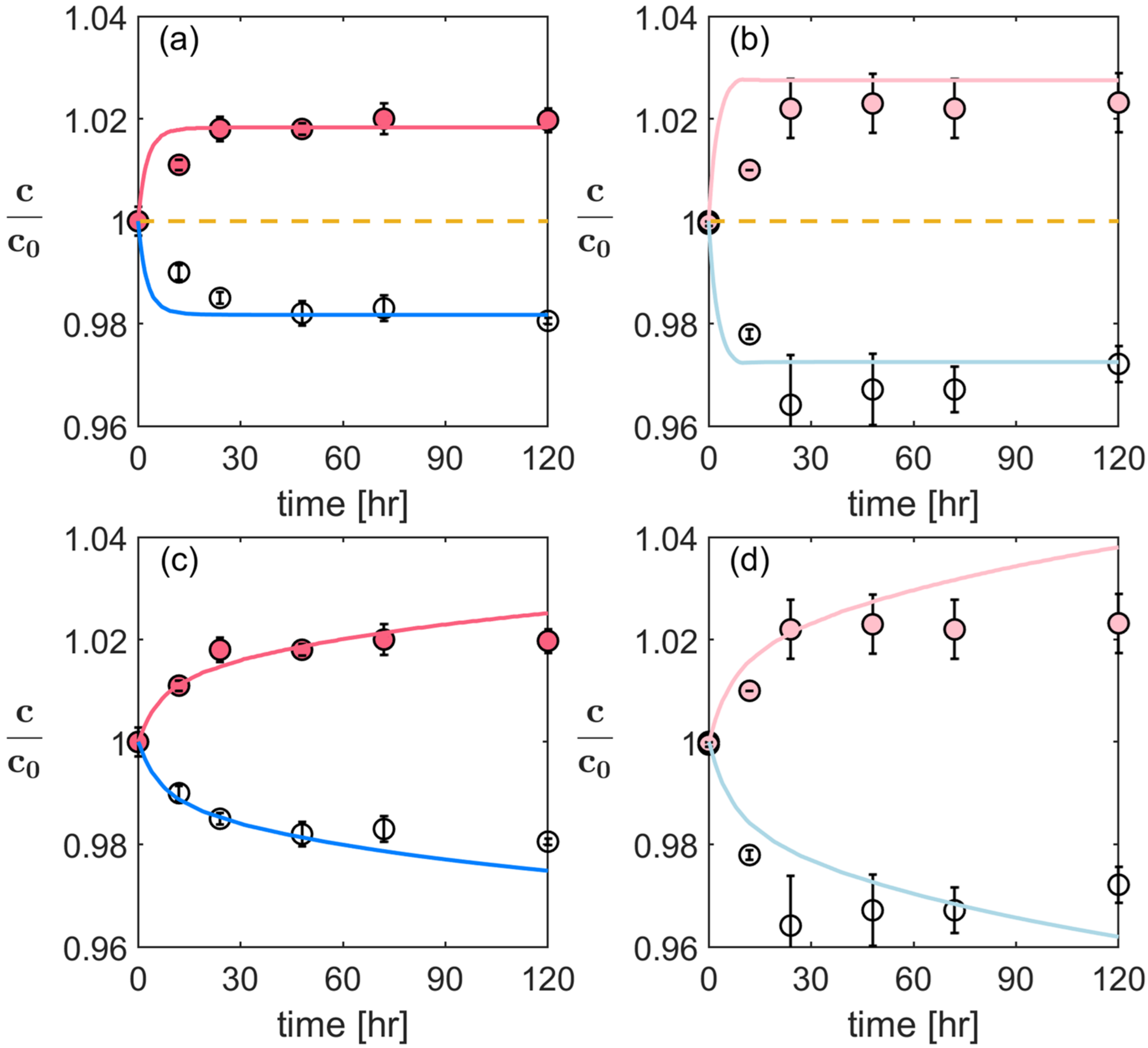

Figure S1: Temporal evolution of $MnCl_2$ as reported in experiments for initial concentration of 10mM (a,c) and 1mM (b,d), and numerical simulations (curves) with a constant cluster size (a,b), and a dynamically evolving cluster size (c,d). Closed symbols correspond to near section and empty symbols are for the far section of the domain.

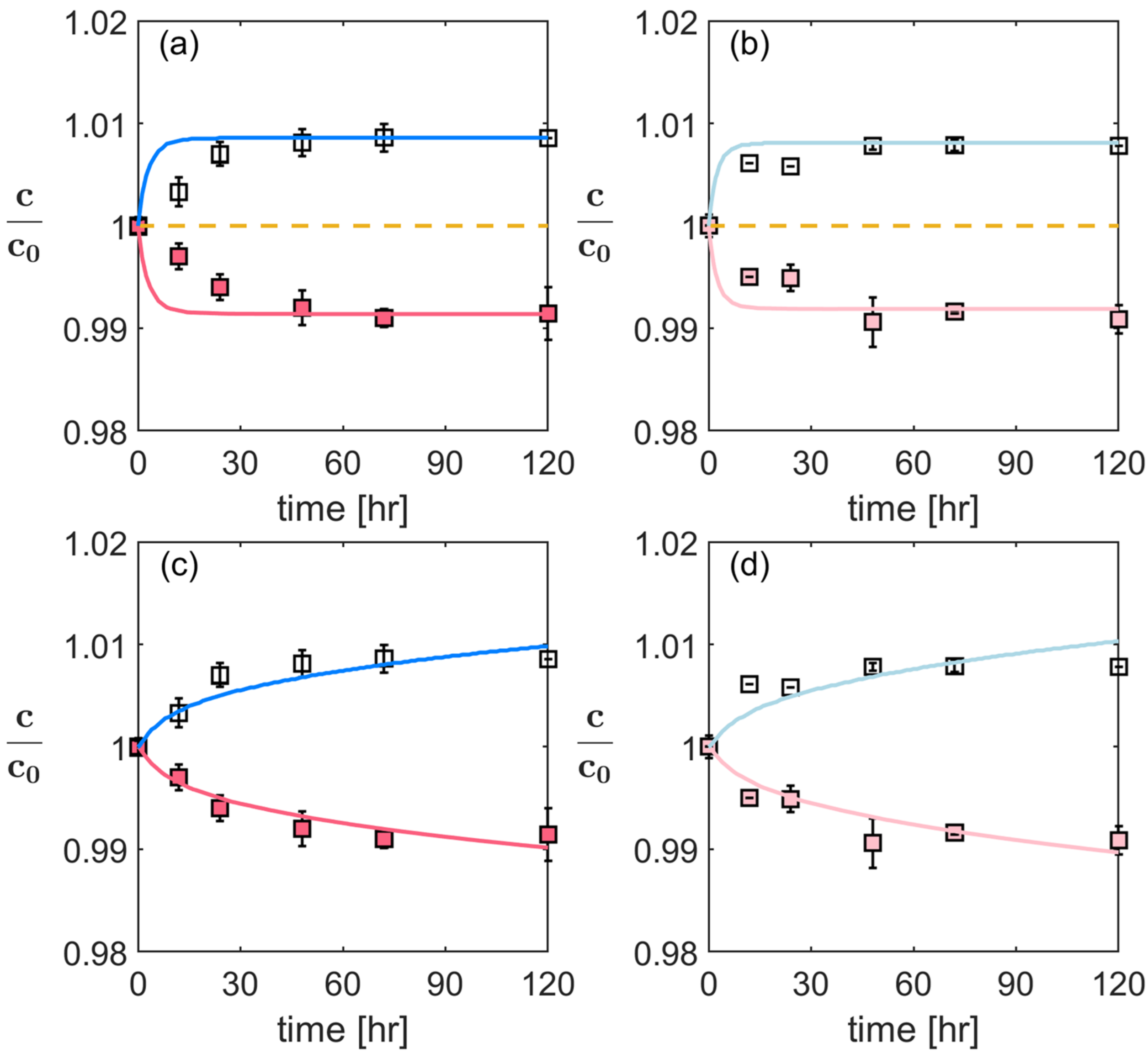

Figure S2: Temporal evolution of $ZnCl_2$ as reported in experiments for initial concentration of 10mM (a,c) and 1mM (b,d), and numerical simulations (curves) with a constant cluster size (a,b), and a dynamically evolving cluster size (c,d). Closed symbols correspond to near section and empty symbols are for the far section of the domain.

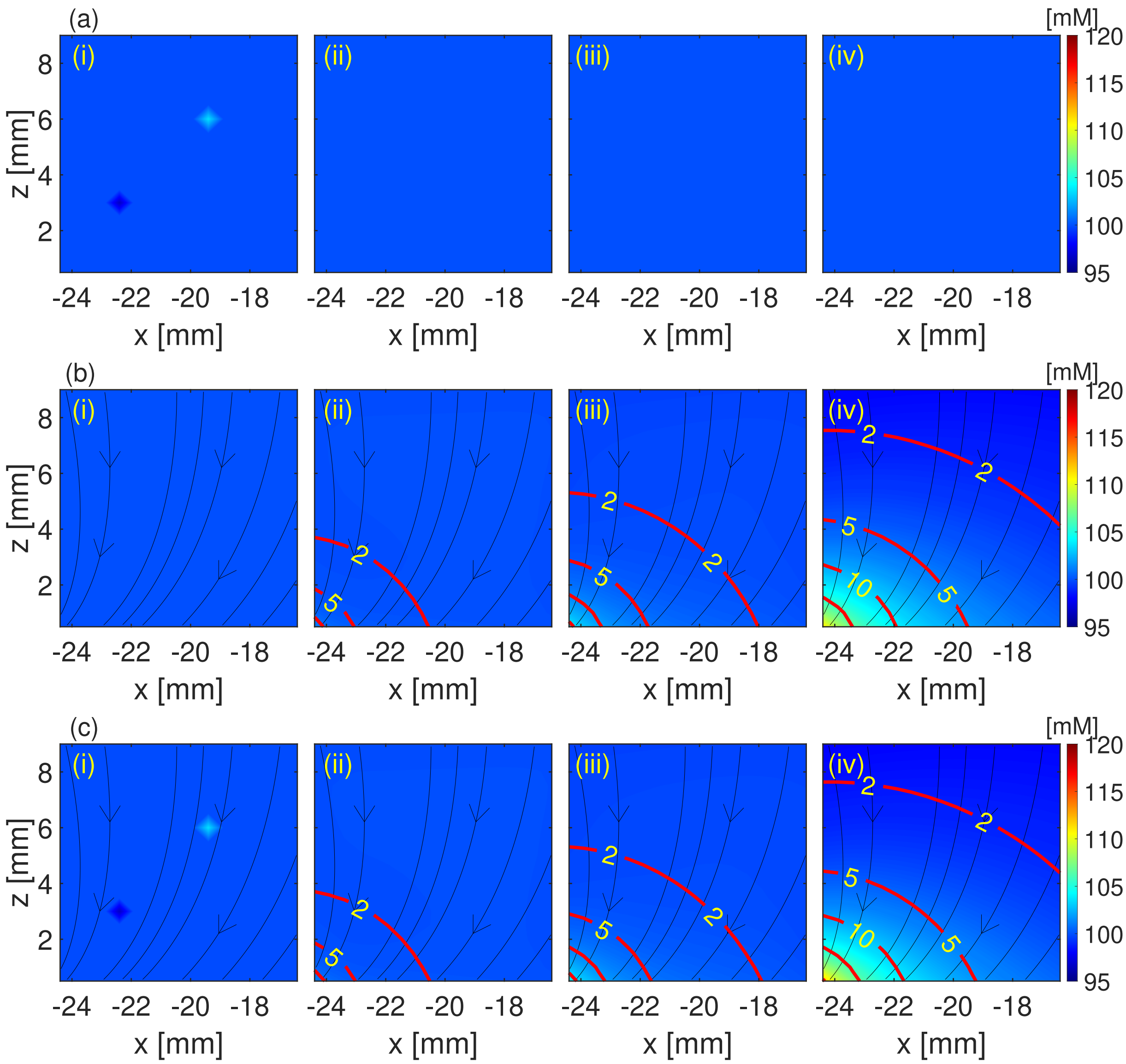

Figure S3: Spatio-temporal evolution of $MnCl_2$ concentration under different magnetic force contributions for an initial concentration of 100 mM. (a) Paramagnetic force only ($F_{\nabla c}$), (b) Kelvin force only ($F_{\nabla B}$), and (c) combined paramagnetic and Kelvin forces. Each subpanel shows heatmaps of concentration along with velocity vectors and contours at four time points: $t = 0$ (i), 0.1 (ii), 1 (iii), and 12 (iv) hours. The color gradients represent ion enrichment toward the magnet. Velocities are shown in nm/s.

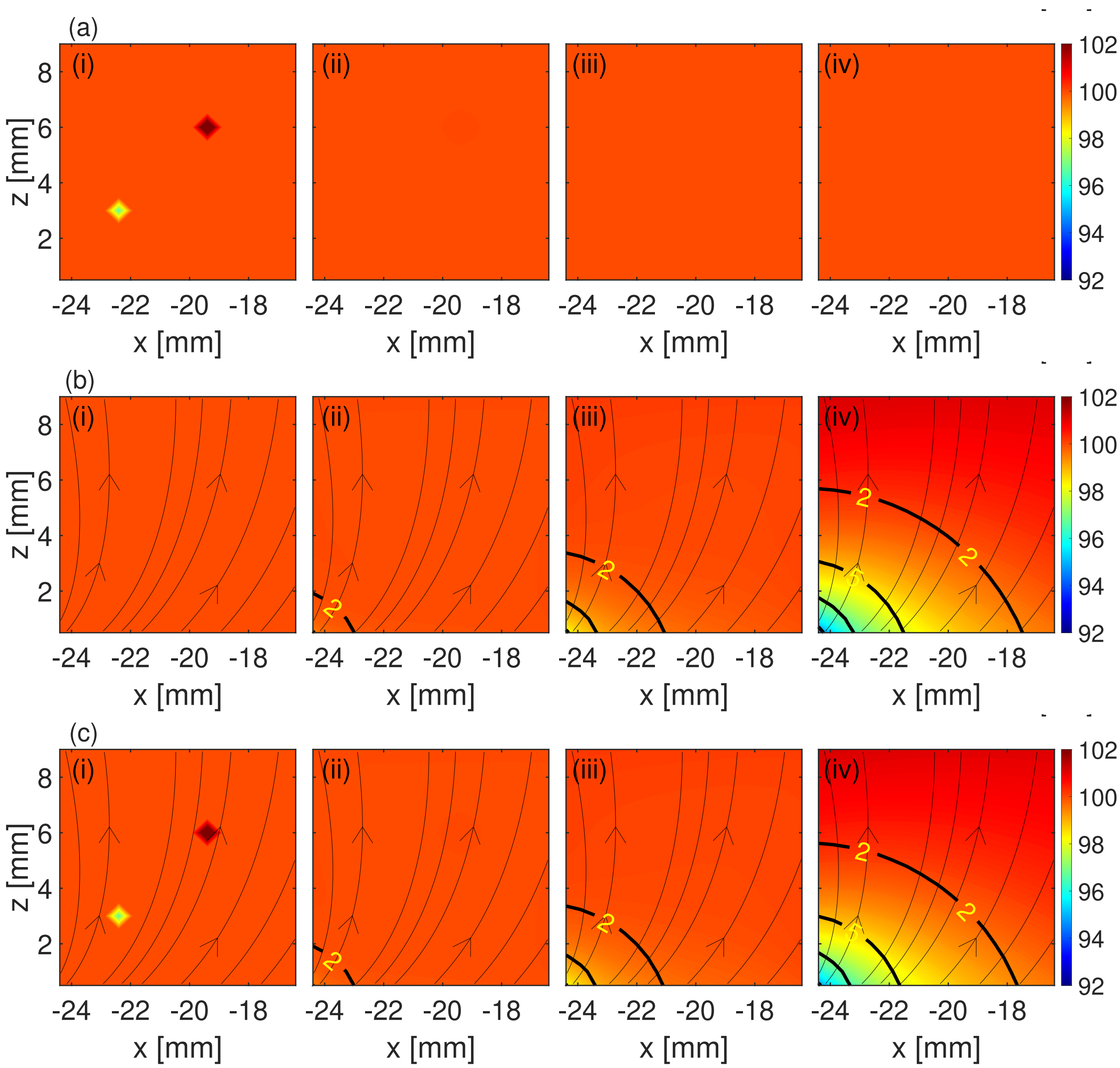

Figure S4: Spatio-temporal evolution of $ZnCl_2$ concentration under different magnetic force contributions for an initial concentration of 100 mM. (a) Paramagnetic force only ($F_{\nabla c}$), (b) Kelvin force only ($F_{\nabla B}$), and (c) combined paramagnetic and Kelvin forces. Each subpanel shows heatmaps of concentration along with velocity vectors and contours at four time points: $t = 0$ (i), 0.1 (ii), 1 (iii), and 12 (iv) hours. The color gradients represent ion depletion toward the magnet. Velocities are shown in nm/s.

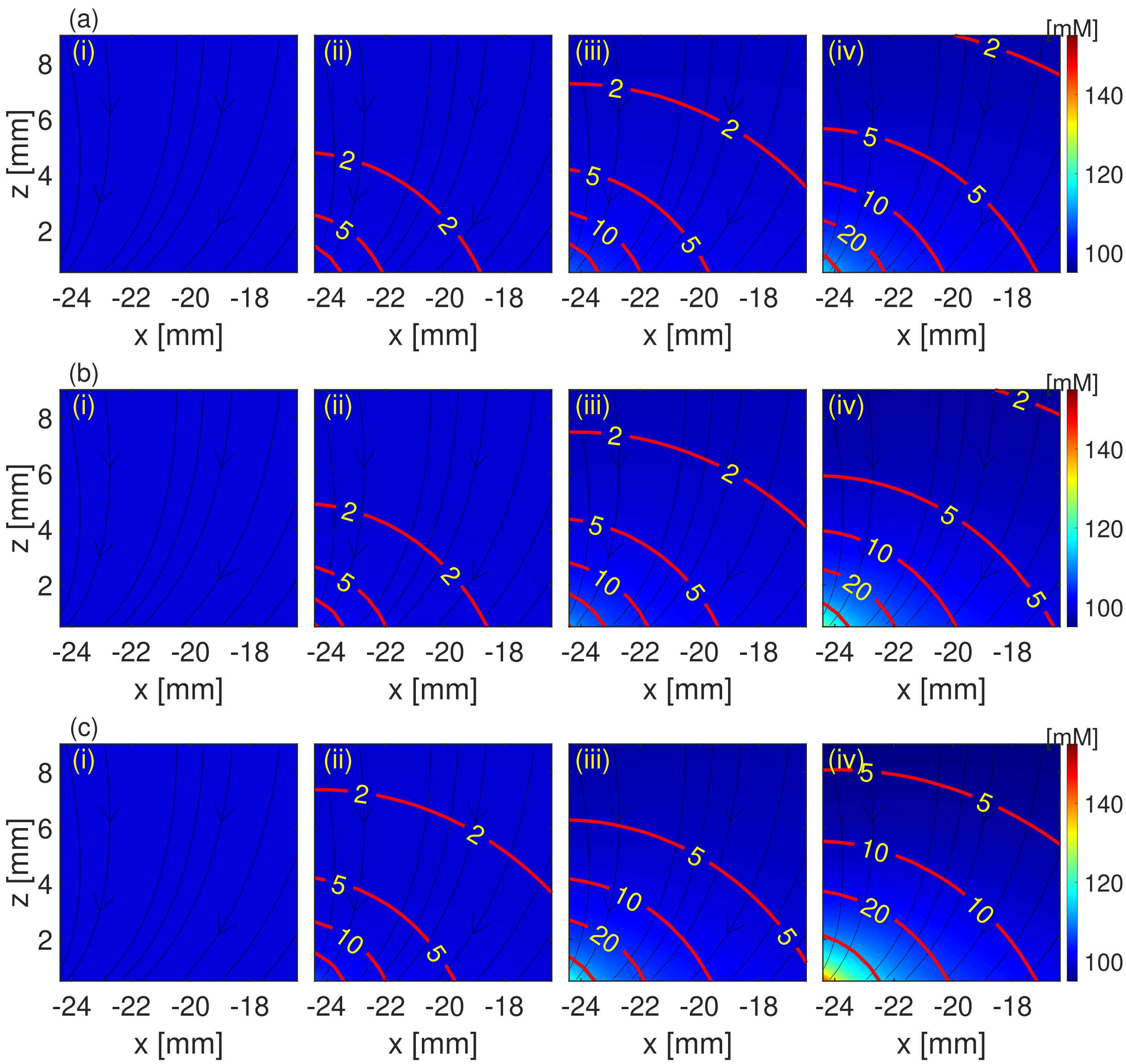

Figure S5: Spatio-temporal evolution of $MnCl_2$ concentration in porous media with an initial concentration of 100 mM, simulated using Brinkman's formulation. Panels correspond to particle sizes of (a) 63 μm, (b) 168 μm, and (c) 500 μm, respectively. Each subpanel presents concentration heatmaps overlaid with velocity vectors and contours at four time points: $t = 0$ (i), 1 (ii), 12 (iii), and 72 (iv) hours. The color gradient represents ion enrichment toward the magnet, and velocities are expressed in nm/s.

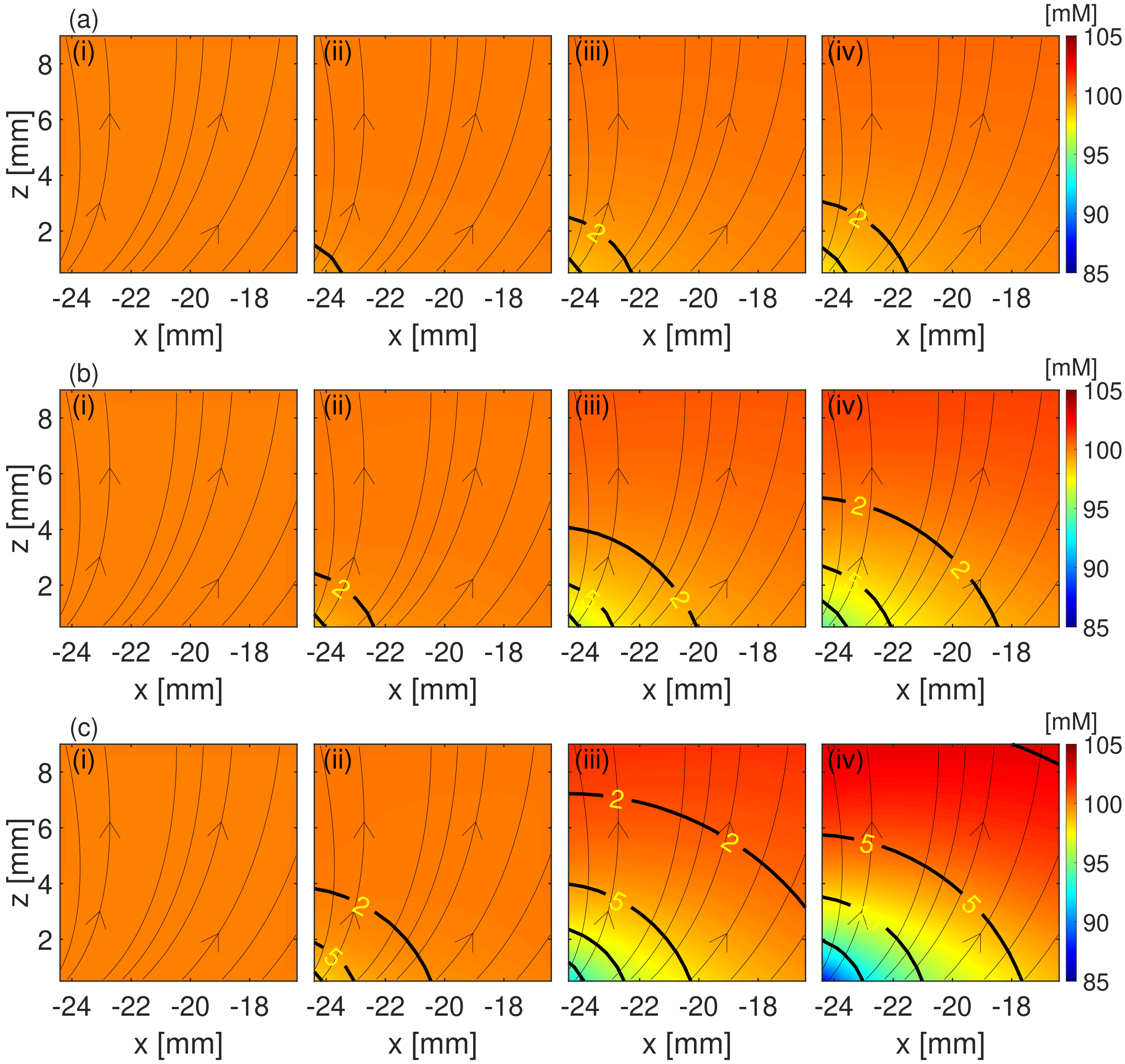

Figure S6: Spatio-temporal evolution of $ZnCl_2$ concentration in porous media with an initial concentration of 100 mM, simulated using Brinkman's formulation. Panels correspond to particle sizes of (a) 63 μm, (b) 168 μm, and (c) 500 μm, respectively. Each subpanel presents concentration heatmaps overlaid with velocity vectors and contours at four time points: $t = 0$ (i), 1 (ii), 12 (iii), and 72 (iv) hours. The color gradient represents ion depletion toward the magnet, and velocities are expressed in nm/s.

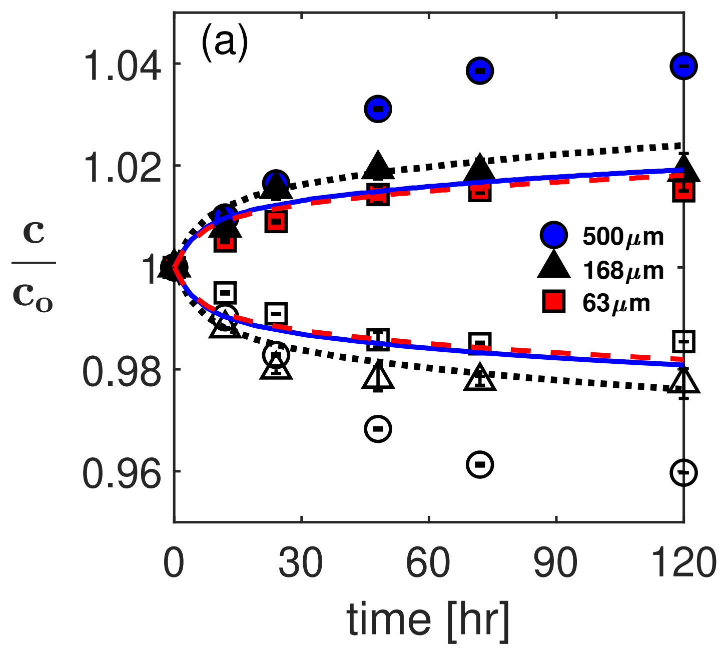

Figure S7: Temporal evolution of normalized $MnCl_2$ concentration in various porous media, along with predictions from the Brinkman formulation (solid curves) using permeability values estimated by the Carman-Kozeny model. In here the red, blue and black curves correspond to porous media with a 63 μm, 500 μm, and a polydisperse (denoted as 168 μm) particle size.

Permeability Measurement Using Darcy's Law

The permeability of the porous media was determined using Darcy's law, as shown in equation below using the experimental setup illustrated in Fig. S8.

$$q = \frac{\kappa}{\mu L}\Delta P \tag{E1}$$

where q is the volumetric flux [m^3/s], κ is the permeability of the porous medium [m^2], μ is the dynamic viscosity of the fluid [Pa·s], $L = 20$ mm is the length of the porous section, and ΔP is the pressure drop across the medium [Pa]. In this setup, a syringe pump delivers water to the inlet of a tube containing the porous medium, with the outlet discharging into a beaker. A differential pressure sensor is connected in parallel at both the inlet and the outlet of the porous section to record the pressure drop without disrupting the flow. To account for system resistance, an initial run was performed without the porous medium to quantify the pressure loss due to tubing and fittings. The value obtained was -188 Pa, which was subtracted from all subsequent readings with the porous media in place.

Measurements were then conducted for the three types of porous media described in the main text: (i) 63 μm monodispersed silica gel, (ii) polydispersed silica gel, and (iii) 500 μm monodispersed silica gel. For each case, pressure drops were recorded at two different volumetric flow rates: 1 mL/min and 3 mL/min. These flow rates enabled the evaluation of permeability under different flux conditions. The pressure drop values were obtained using computer software and are shown in black in Fig. (S9). To determine the average pressure drop, the raw data were smoothed by averaging, resulting in a straight trend line displayed in blue. The corresponding permeability values, calculated from the averaged pressure drops, are presented in Table S1.

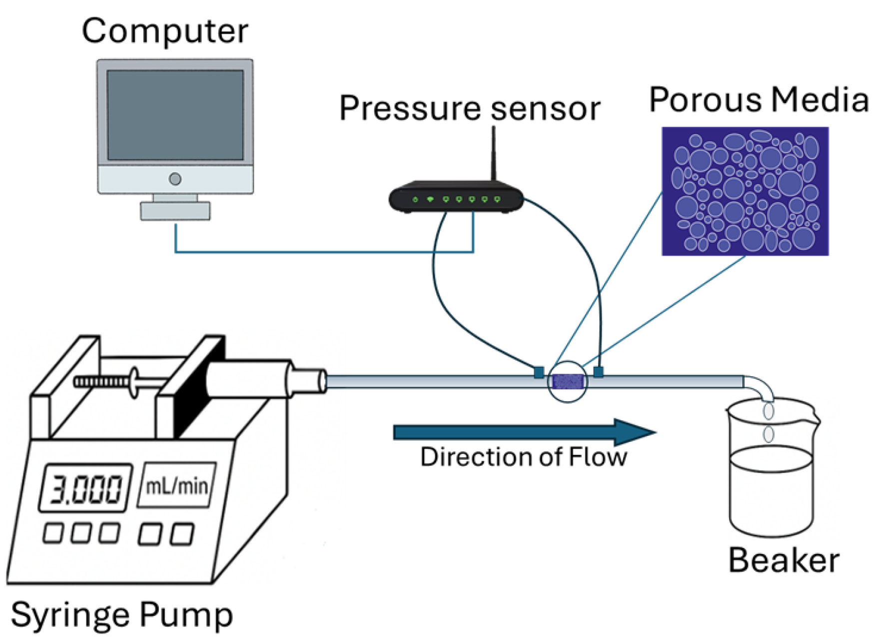

Figure S8: A schematic of the experimental setup used for permeability measurements of various porous media.

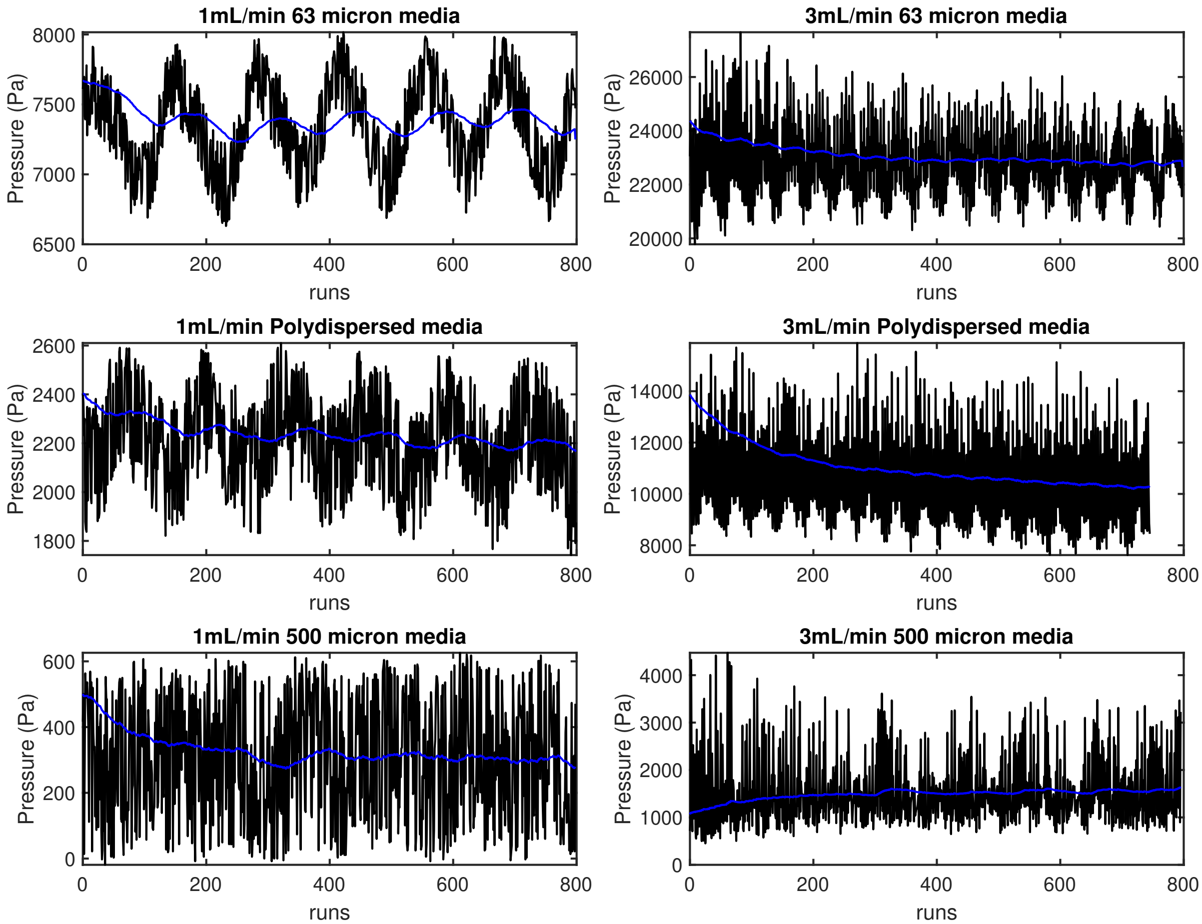

Figure S9: Pressure drop measurement for permeability in different porous media

Table S1: List of experimentally measured parameters for determining the permeability of the porous medium used in this study

Porous media	Flow rate [mL/min]	Pressure drop ΔP [Pa]	Permeability $\kappa \times 10^{12} [m^2]$
polydispersed	1	2431	8.73
	3	10742	5.93
63 μm	1	7581	2.80
	3	24052	2.70
500 μm	1	517	41.08
	3	1672	38.07